

<sup>4)</sup>The inequality (4.1) can be regarded as a restriction on the efficiency  $\eta$  of the crystal in the current-source regime,  $\eta_{\max} < 1$ .

- <sup>1</sup>V. I. Belinicher, V. K. Malinovskii, and B. I. Sturman, Zh. Eksp. Teor. Fiz. 73, 692 (1977) [Sov. Phys. JETP 46, 362 (1977)].  
<sup>2</sup>V. I. Belinicher and B. I. Sturman, Fiz. Tverd. Tela (Lenigrad) 20, 821 (1978) [Sov. Phys. Solid State 20, 476 (1978)].  
<sup>3</sup>E. M. Baskin, M. D. Bloch, M. V. Entin, and L. I. Magarill, Phys. Status Solidi B 83, K97 (1977).  
<sup>4</sup>V. M. Galitskii, S. P. Goreslavskii, and V. F. Elesin, Zh. Eksp. Teor. Fiz. 57, 207 (1969) [Sov. Phys. JETP 30, 117 (1970)].  
<sup>5</sup>S. P. Goreslavskii and V. F. Elesin, Voprosy teorii atomnykh stolknovenii (Topics in the Theory of Atomic Collisions), Atomizdat, 1970, p. 157.  
<sup>6</sup>L. D. Landau and E. M. Lifshitz, Kvantovaya mekhanika

- (Quantum Mechanics), Nauka, 1974 [Pergamon 1977].  
<sup>7</sup>N. V. Genkin and P. M. Mednis, Zh. Eksp. Teor. Fiz. 54, 1137 (1968) [Sov. Phys. JETP 27, 609 (1969)].  
<sup>8</sup>V. I. Belinicher, Phys. Lett. A 66, 213 (1978).  
<sup>9</sup>W. Heitler, The Quantum Theory of Radiation, Oxford, 1954.  
<sup>10</sup>F. Bertin, Principles of Quantum Electronics (Russ. Transl.), Mir, 1971.  
<sup>11</sup>E. Schrödinger, Phys. Rev. 182, 632 (1969).  
<sup>12</sup>A. S. Davydov, Teoriya tverdogo tela (Solid State Theory), Nauka, 1976.  
<sup>13</sup>V. F. Elesin, Zh. Eksp. Teor. Fiz. 69, 572 (1975) [Sov. Phys. JETP 42, 291 (1975)].  
<sup>14</sup>A. M. Glass, Von der Linde, and T. J. Negrane, Appl. Phys. Lett. 25, 233 (1974).  
<sup>15</sup>L. D. Landau and E. M. Lifshitz, Elektrodinamika sploshnykh sred (Electrodynamics of Continuous Media), Fizmatgiz, 1959 [Pergamon, 1960].

Translated by J. G. Adashko

## Hyper-Raman scattering in an LiNbO<sub>3</sub> crystal

V. N. Denisov, B. N. Mavrin, V. B. Podobedov, and Kh. E. Sterin

Institute of Spectroscopy, Academy of Sciences of the USSR, Troitsk, Moscow Province  
(Submitted 2 March 1978)

Zh. Eksp. Teor. Fiz. 75, 684–690 (August 1978)

It was found that the hyper-Raman scattering of light can be observed even in noncentrosymmetric crystals if the exciting radiation travels along a direction for which there was no phase matching. A multichannel photoelectric recording system was used in an investigation of the hyper-Raman spectra of crystalline LiNbO<sub>3</sub> in various scattering geometries. The time taken to record spectra in the 0–900 cm<sup>-1</sup> range did not exceed 12 min. The E vibrations dominated the spectra in the investigated geometries. Estimates were obtained of the scattering cross section and nonlinear susceptibility in the hyper-Raman scattering in LiNbO<sub>3</sub>.

PACS numbers: 78.30.Gt, 42.65.Cq, 07.62.+s

### INTRODUCTION

1. The hyper-Raman scattering (HRS) of light is a three-photon process in which a system interacts with two photons of frequency  $\nu_0$  and emits one photon at a frequency  $2\nu_0 \pm \nu_{ph}$  ( $\nu_{ph}$  is the frequency of an optical phonon). The HRS is a quadratic term in the expansion of the polarization  $P$  of a medium as a series in powers of the field intensity  $E$  of the exciting wave:

$$P = \alpha E + \beta E^2 + \dots \quad (1)$$

The hyperpolarizability  $\beta$  is much less than the polarizability  $\alpha$ . Therefore, the HRS can only be observed in sufficiently strong fields. The activity of vibrations in the HRS is governed by a rank-four hyperpolarizability tensor and it may be found that vibrations which do not participate in the spontaneous Raman scattering or in infrared absorption can take part in the HRS.<sup>[1,2]</sup> The HRS spectra have been recorded for gases, liquids, and solids.<sup>[3,4]</sup>

Although the HRS was discovered over 10 years ago,<sup>[5]</sup> it has been observed in just four noncentrosymmetric solids: fused quartz,<sup>[5]</sup> crystals of NH<sub>4</sub>Cl,<sup>[6]</sup> diamond,<sup>[7]</sup> and CsI (Ref. 8). It is difficult to observe the HRS in noncentrosymmetric crystals because of the possible generation of the second harmonic of the ex-

citing radiation  $\nu_0$  which may then give rise to the spontaneous Raman scattering in the same part of the spectrum as the HRS. We shall use the example of a non-linear LiNbO<sub>3</sub> crystal to show that, if the exciting radiation travels along a direction for which there is no second-harmonic phase matching, the HRS can also be easily observed in a noncentrosymmetric crystal.

Crystals of LiNbO<sub>3</sub> have lower damage thresholds than those of the materials investigated earlier.<sup>[5–8]</sup> Therefore, we restricted the density of the exciting radiation to  $\leq 10^8$  W/cm<sup>2</sup>. Use was made of a multichannel photoelectric recording system by means of which we were able to obtain weak HRS spectra of LiNbO<sub>3</sub> at a relatively low exciting radiation density. The scattering cross sections and nonlinear susceptibility in the HRS process were determined for this crystal.

### DESCRIPTION OF EXPERIMENTS

We used the apparatus shown schematically in Fig. 1. The HRS spectra of an LiNbO<sub>3</sub> crystal were excited by the  $\lambda = 1064$  nm line of a pulsed YAG laser 1 ( $I_0 \approx 2 \times 10^4$  W,  $\tau_p \sim 10^{-8}$  sec, divergence  $\sim 10^{-3}$  rad, pulse repetition frequency 25 Hz). The spontaneous Raman scattering spectra of the crystal were excited under similar con-

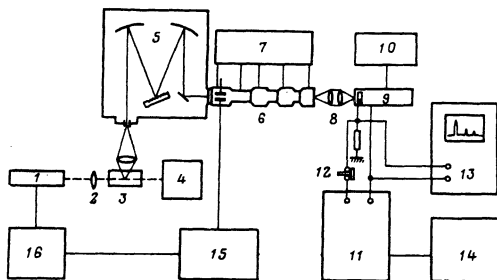


FIG. 1. Schematic diagram of the apparatus: 1) pulsed YAG laser; 2), 8) objectives; 3) crystal; 4) average-power meter; 5) spectrograph; 6) image converter; 7) power supply of the image converter; 9) vidicon camera tube; 10) control and power supply units of the vidicon; 11) multichannel digital storage unit; 12) switch for isolating storage unit; 13) oscilloscope; 14) recording potentiometer; 15) generator of gate pulses applied to the converter; 16) control and supply units of the laser.

ditions by the second harmonic of the same laser. The average power of the exciting radiation ( $\nu_0$  or  $2\nu_0$ ) passing through the crystal 3 was monitored by a thermocouple meter 4 and kept below the dielectric breakdown threshold of  $\text{LiNbO}_3$ . The radiation scattered at an angle of  $90^\circ$  was collected from a solid angle of  $\sim 0.13 \text{ sr}$  and analyzed with a spectrograph 5. An improved variant of a multichannel photoelectric recording system<sup>[9]</sup> was used; it was based on an image converter 6, television camera tube 9, and multichannel digital storage unit 11. The most important properties of the system were its multichannel nature, i.e., ability to record simultaneously a part of the spectrum  $\sim 600 \text{ cm}^{-1}$  wide, and a low noise of the input stage of the image converter ( $\sim 1$  photoelectron per 10 sec per resolvable element). The last feature was ensured by gating the normally shut-off first chamber of the image converter by pulses synchronized with the laser radiation. In this way, the noise due to the first photocathode of the converter was reduced by a factor of  $\sim 10^5$ .

Accumulation of spectral data produced by a large (up to  $10^4$ ) number of laser pulses took place in two stages. The preliminary accumulation in  $\sim 8$  sec took place on the target of the vidicon camera tube 9. The spectrum accumulated in this way was then read out in  $\sim 0.1$  sec and applied to the multichannel storage unit. The final spectrum was obtained after repeating many times the complete accumulation cycle and it was displayed on the screen of an oscilloscope 13 in the course of an experiment. This method of data acquisition made it possible to reject the cycles during which there were intense disturbances as a result of dielectric breakdown in the crystal. The rejected spectrum was not passed on to the storage unit and was erased from the vidicon target, and the next accumulation cycle was started by using a different, undamaged part of the crystal.

The HRS and spontaneous Raman spectra of the  $\text{LiNbO}_3$  crystal were recorded in the  $0\text{--}950 \text{ cm}^{-1}$  range. The reciprocal linear dispersion of our spectrograph was  $2.5 \text{ nm/mm}$  so that a spectral region of  $\sim 600 \text{ cm}^{-1}$  could be recorded simultaneously. Therefore, the whole spectrum was covered in two stages:  $0\text{--}500$  and

$400\text{--}900 \text{ cm}^{-1}$ . The two stages were then matched using the common lines in the overlapping interval  $400\text{--}500 \text{ cm}^{-1}$ . A complete HRS spectrum ( $0\text{--}950 \text{ cm}^{-1}$ ) was recorded under 12 min. The line frequencies in the HRS and spontaneous Raman spectra were determined by linear interpolation between the known frequencies of the  $2\nu_0$  line and the emission line of Ne in the  $500\text{--}560 \text{ nm}$  range.

The height of the illuminated region in the crystal, from which the scattered radiation was collected, was set by the parameters of the recording system and amounted to 4 mm. It was selected to be slightly less than the length of the equivalent cylinder (length of the constriction)<sup>[10]</sup> within which the nonlinear HRS process was most effective. This selection made it possible to carry out a reliable comparison of the intensities of the HRS and spontaneous Raman lines.

The HRS spectra were excited in an oriented crystal of  $\text{LiNbO}_3$  whose dimensions were  $20 \times 15 \times 30 \text{ mm}$ . The primitive cell of this crystal had the spatial symmetry  $C_{3v}^6$  and contained two formula units. The optical vibrations were as follows:  $4A_1 + 5A_2 + 9E$ , of which the  $A_1$  and  $E$  vibrations were active in the stimulated Raman scattering, infrared absorption, and HRS, and  $A_2$  was only active in the HRS.

In the transparency region of a crystal, the spontaneous Raman and HRS scattering tensors are symmetric and should not have more than six and nine independent components, respectively. The nonvanishing components of these tensors are listed for  $\text{LiNbO}_3$  in Tables I and II. The components of the spontaneous Raman tensor  $\alpha_{ij}$  ( $i, j = x, y, z$ ) govern the intensity of the spontaneously scattered light in the geometry in which the incident light is polarized along the  $i$  axis and the scattered light along the  $j$  axis. In the HRS process, a crystal is excited by two photons and emits one photon. Therefore, a component  $\beta_{ijk}$  of the HRS tensor governs the HRS intensity when the geometry is such that one of the exciting photons is polarized along the  $i$  axis, the other along the  $j$  axis, and the scattered photon along the  $k$  axis. Nine out of ten components of the HRS tensor correspond to the case when both photons are polarized in the same way (Table I). Our experiments were confined to the cases of identical polarization of the exciting photons, so that the geometries in HRS and spontaneous Raman scattering could be designed in the same way.

The components of the spontaneous Raman scattering tensor of uniaxial crystals obey the relationships  $|\alpha_{xx}| = |\alpha_{yy}| = |\alpha_{xy}|$  and  $|\alpha_{yz}| = |\alpha_{xz}|$ . Hence, it follows that we cannot distinguish the  $x$  and  $y$  axes on the

TABLE I. Spontaneous scattering tensor.

	$\alpha_{xx}$	$\alpha_{yy}$	$\alpha_{zz}$	$\alpha_{yz}$	$\alpha_{xz}$	$\alpha_{xy}$
$E(x)$	$c$	$-c$		$d$		
$E(y)$					$d$	$c$
$A_1(z)$	$a$	$a$	$b$			

TABLE II. Hyper-Raman scattering tensor.

	$\beta_{xxx}$	$\beta_{yuu}$	$\beta_{zzz}$	$\beta_{xxv}$	$\beta_{yyz}$	$\beta_{zxx}$	$\beta_{xzx}$	$\beta_{yyx}$	$\beta_{xzu}$	$\beta_{xuz}$
$E(x)$	$d'$				$e'$	$f'$	$-e'$	$d'/3$		$e'$
$E(y)$		$d'$		$d'/3$		$c'$		$-a'$	$f'$	
$A_1(z)$	$a'$		$b'$		$-b'$					
$A_2$		$b'$								

basis of spontaneous scattering. However, in the case of the HRS tensor, the  $x$  and  $y$  axes are no longer equivalent (Table II) and the correct interpretation of the HRS spectra requires knowledge of the directions of the  $x$  and  $y$  axes.

The propagation of an intense laser beam of frequency  $\nu_0$  in a nonlinear  $\text{LiNbO}_3$  crystal always excites the second harmonic  $2\nu_0$ , whose intensity depends on the direction of propagation. In this crystal, the direction of phase-matched second-harmonic generation is close to the  $xy$  plane ( $\theta \approx 84^\circ$ ). When the  $\nu_0$  beam travels along the  $xy$  plane, the intensity of the second harmonic is high enough for the spontaneous Raman spectrum excited by this harmonic to be stronger than the HRS spectrum. Therefore, we investigated HRS in the scattering geometries such that the exciting beam was directed along the  $z$  axis. The second harmonic, which was then excited in  $\text{LiNbO}_3$ , was polarized along the  $x$  axis.<sup>[11]</sup>

For a laser beam of frequency  $\nu_0$  traveling along the  $z$  axis, certain vibration modes may appear in the infrared spectra, depending on the scattering geometry (Table II). For the  $z(yy)x$  and  $z(xy)x$  geometries, we find that the relevant vibration modes are  $E_T + A_2$ ; for  $z(yz)x$  and  $z(xz)x$ , we obtain  $E_m + A_m$ ; for  $z(xz)y$ ,  $z(xx)y$ ,  $z(yx)y$ , and  $z(yz)y$ , the result is  $E_T + A_m$  ( $T$  denotes the transverse vibrations and  $A_m$  the mixed vibrations).

## RESULTS AND DISCUSSION

A comparison of the HRS and spontaneous Raman spectra demonstrates that excitation with light of frequency  $\nu_0$  generates the HRS and not the spontaneous spectra in the frequency range  $2\nu_0 - \nu_{ph}$ . We shall consider the HRS spectra obtained in the  $z(yx)y$  geometry when the  $E_T + A_m$  vibrations are active. For a beam of frequency  $\nu_0$  directed along the  $z$  axis, we may expect excitation of the second harmonic  $2\nu_0$  of the beam polarized along the  $x$  axis. The spontaneous Raman spectrum excited by the second harmonic corresponds to the  $z(xx)y$  geometry when, again, the  $E_T + A_m$  vibrations are active.

For comparison, curve 1 in Fig. 2 shows the spontaneous Raman scattering spectrum obtained in the  $z(xx)y$  geometry. However, excitation with the fundamental frequency  $\nu_0$  produces a spectrum (curve 2 in Fig. 2) which differs from the spontaneous spectrum (curve 1 in Fig. 2). For example, the strongest line in the spontaneous spectrum (curve 1 in Fig. 2) is located

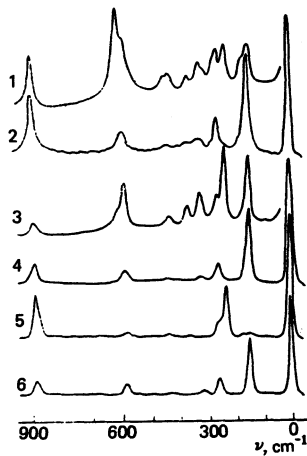


FIG. 2. Spontaneous Raman and HRS spectra of  $\text{LiNbO}_3$ . Geometry in spontaneous scattering: 1)  $z(xx)y$ ; 3)  $z(xz)y$ . Geometry in HRS: 2)  $z(yx)y$ ; 4)  $z(xx)y$ ; 5)  $z(xz)x$ ; 6)  $z(xy)x$ .

at  $607 \text{ cm}^{-1}$  ( $A_m$  vibration) but this line is practically absent from the spectrum (curve 2 in Fig. 2). Another characteristic of the spectrum represented by curve 2 in Fig. 2 is that the intensity of the  $2\nu_0$  line is comparable with the intensities of other lines in the spectrum. On the other hand, in the spontaneous spectrum, the intensity of the  $2\nu_0$  line is approximately 100 times greater than the intensities of the other lines. These features of the spectrum represented by curve 2 in Fig. 2 indicate that it is not due to the spontaneous Raman scattering.

This conclusion is additionally supported by a quantitative analysis of the intensity of the  $151 \text{ cm}^{-1}$  line in the spectra represented by curves 1 and 2 in Fig. 2 and of the intensity of the second harmonic along the  $z$  axis. The intensity scale of our system was calibrated first in photons per second per resolvable element. All the measurements were carried out at a fixed power of the incident light ( $I_0 = 2 \times 10^4 \text{ W}$ ). The intensity of the second harmonic along the direction of the exciting light (along the  $z$  axis) was  $\sim 10^{-9} I_0$ . The intensity of the  $151 \text{ cm}^{-1}$  line measured for the same solid collection angle was  $\sim 4 \times 10^{-10} I_0$  in the spontaneous spectrum (curve 1 in Fig. 2) and  $\sim 2 \times 10^{-14} I_0$  in the other spectrum (curve 2 in Fig. 2). These results indicated that, in the case of excitation of the latter spectrum (curve 2 in Fig. 2) by the second harmonic, the intensity of the  $151 \text{ cm}^{-1}$  line would not have exceeded  $\sim 10^{-19} I_0$ . In fact, we found a signal which was  $\sim 10^5$  times as strong.

Finally, a study of the spectrum of the radiation along the direction of the exciting beam (forward direction) demonstrated a small contribution of the cascade processes, including the stimulated Raman scattering, to the intensity of the spectra represented by curves 2 and 4–6 in Fig. 2. The spectral composition of the radiation in the forward direction was determined in the frequency interval from  $2\nu_0$  to  $2\nu_0 - 900 \text{ cm}^{-1}$ . It was found that the intensity of the  $2\nu_0$  line was at least  $10^3$  times higher than the intensities of the  $2\nu_0 - \nu_{ph}$  lines, which could have been due to the addition of the stimulated Raman scattering frequencies  $\nu_0 - \nu_{ph}$  and of the exciting radiation  $\nu_0$ . The stimulated Raman scattering at the  $\nu_0 - \nu_{ph}$  frequency traveled in the forward or back-

ward direction, i.e., it could also travel opposite to the exciting radiation. According to the law of conservation of momentum, the radiation at the  $2\nu_0 - \nu_{ph}$  frequency should be directed forward, like the second harmonic  $2\nu_0$ , irrespective of the direction of stimulated Raman scattering. Scattering by inhomogeneities in the investigated crystal could result in the observation of the  $2\nu_0 - \nu_{ph}$  radiation at a scattering angle of  $90^\circ$ . However, its intensity, like that along the  $z$  axis, could not exceed  $10^{-3}$  of the intensity of the  $2\nu_0$  line in the spectra shown in Fig. 2 (curves 2 and 4–6).

The reported results allow us to conclude that, in the case of a laser beam of frequency  $\nu_0$  directed along the  $z$  axis, we observed the HRS and not the spontaneous Raman spectra.

As expected, the intensity of the HRS lines was a quadratic function of the exciting intensity  $I_0$ . The observed intensity of the HRS line at  $151\text{ cm}^{-1}$  ( $E_T$  vibration, curve 2 in Fig. 2) represented only one photon per five laser pulses when the exciting intensity was  $I_0 = 2 \times 10^4\text{ W}$ .

The HRS spectra obtained in the investigated geometries had other special features. They showed particularly the  $E$  vibrations (curves 2 and 4–6 in Fig. 2). This was established by comparing the spontaneous Raman spectrum of the  $E_T$  vibrations (curve 3 in Fig. 2) with the HRS spectra in which the  $E_T + A_m$  (curves 2 and 4 in Fig. 2) and  $E_T + A_2$  (curve 6 in Fig. 2) vibrations were active. The intensity of the  $A_m$  vibrations in the HRS spectra was low. The forbidden (in the infrared absorption and spontaneous Raman spectra)  $A_2$  vibrations could appear in the HRS only in combination with the  $E$  vibrations (Table II). However, in the scattering geometry in which the  $E_T + A_2$  vibrations were HRS-active (curve 6 in Fig. 2), only the  $E_T$  vibrations were observed. Therefore, either the  $A_2$  and  $E_T$  vibration frequencies were close (the resolution of the apparatus was  $\sim 20\text{ cm}^{-1}$ ) or the intensity of the  $A_2$  vibrations was also low in the HRS.

We shall now estimate the cross section and nonlinear susceptibility of the HRS process for the  $151\text{ cm}^{-1}$  line. The HRS intensity can be represented in the form

$$I_{HRS} = \sigma_{HRS} l \frac{\Delta\Omega}{n^2} N_v I_0 [\text{W}] \quad (2)$$

Here,  $\sigma_{HRS}$  is the cross section ( $\text{cm}^2 \cdot \text{cell}^{-1} \cdot \text{sr}^{-1}$ ),  $l$  is the length (cm),  $\Delta\Omega$  is the solid angle of collection of the scattered light (sr),  $n$  is the refractive index,  $N_v$  is the number of primitive cells per  $1\text{ cm}^3$ , and  $I_0$  is the intensity of the exciting radiation (W). The HRS cross section is estimated by comparing the intensities of the spontaneous Raman and HRS lines. The value of  $I_{HRS}$  for  $I_0 = 2 \times 10^4\text{ W}$  is given above. Since  $\sigma_{SRS} = 4 \times 10^{-29}\text{ cm}^2 \cdot \text{cell}^{-1} \cdot \text{sr}^{-1}$  for the  $z(xy)x$  geometry,<sup>[12]</sup> we find that  $\sigma_{HRS} = 2 \times 10^{-33}\text{ cm}^2 \cdot \text{cell}^{-1} \cdot \text{sr}^{-1}$  for the  $z(yx)y$  geometry. In contrast to the spontaneous Raman cross section, the HRS value is proportional to the incident radiation density:  $\sigma_{HRS} = \text{const} \times I_0/s$ , where  $s$  is the beam cross section. For our value of  $I_0$  and  $s = 0.3 \times 10^{-4}\text{ cm}^2$ , we find that  $\sigma_{HRS} = 1.6 \times 10^{-42} I_0/s \text{ cm}^2 \cdot \text{cell}^{-1} \cdot \text{sr}^{-1}$ .

$\cdot \text{sr}^{-1}$ .

The intensity of the hyper-Raman scattering by phonons is proportional to the average square of the nonlinear polarization  $p^n$  (Refs. 13 and 14):

$$I_{HRS} \propto (2\nu_0 - \nu_{ph})^4 \langle |P^n|^2 \rangle = (2\nu_0 - \nu_{ph})^4 \chi_{HRS}^2 E_0^4 \langle |Q|^2 \rangle N_v^2 [\text{W}] \quad (3)$$

Here,  $\chi_{HRS} = (\partial\beta/\partial Q)_0$  is the nonlinear susceptibility of the HRS process per cell,  $Q$  is the amplitude of a normal vibration, and  $E_0$  is the intensity of the exciting field (cgs esu). Similarly, we can represent the intensity of the spontaneous Raman scattering excited by the frequency  $2\nu_0$ :

$$I_{SRS} \propto (2\nu_0 - \nu_{ph})^4 \chi_{SRS}^2 E_0^4 \langle |Q|^2 \rangle N_v^2, \quad \chi_{SRS} = (\partial\alpha/\partial Q)_0 \quad (4)$$

Then, we find from Eqs. (3) and (4) that

$$\chi_{HRS} = \chi_{SRS} \left( \frac{I_{HRS}}{I_{SRS}} \right)^{1/2} \frac{1}{E_0} \quad (5)$$

In our case,  $E_0 = 2.4 \times 10^3$  cgs esu. Then, in the case of the  $151\text{ cm}^{-1}$  line, we have

$$\chi_{HRS} \approx 3 \cdot 10^{-6} \chi_{SRS}$$

The nonlinear susceptibility in the spontaneous Raman scattering is related to the spontaneous Raman cross section, as follows:<sup>[15]</sup>

$$\sigma_{SRS} = \frac{\hbar \nu_0^4 N_v}{\pi \rho c^4 \nu_{ph}} (N(\nu_{ph}) + 1) |\chi_{SRS}|^2, \quad (6)$$

where  $\rho$  is the density of the crystal ( $\text{g/cm}^3$ ) and  $N(\nu_{ph})$  is the population factor. We find from Eq. (6) that the susceptibility in spontaneous Raman scattering is  $\chi_{SRS} = 8.4 \times 10^{-17}\text{ cm}^2$ . We then obtain  $\chi_{HRS} \approx 2.5 \times 10^{-22}\text{ cm}^2/\text{cgs esu}$ .

For other lines in the spectrum of the  $\text{LiNbO}_3$  crystal, the values of  $\sigma_{HRS}$  and  $\chi_{HRS}$  can be estimated from the ratios of the intensities in the HRS spectrum (curve 2 in Fig. 2).

<sup>1</sup>S. J. Cyvin, J. E. Rauch, and J. C. Decius, *J. Chem. Phys.* **43**, 4083 (1965).

<sup>2</sup>J. H. Christie and D. J. Lockwood, *J. Chem. Phys.* **54**, 1141 (1971).

<sup>3</sup>D. A. Long, *Adv. Raman Spectrosc.* **1**, 1 (1973).

<sup>4</sup>M. J. French and D. A. Long, *Mol. Spectrosc.* **4**, 225 (1976).

<sup>5</sup>R. W. Terhune, P. D. Maker, and C. M. Savage, *Phys. Rev. Lett.* **14**, 681 (1965).

<sup>6</sup>C. M. Savage and P. D. Maker, *Appl. Opt.* **10**, 965 (1971).

<sup>7</sup>W. Yu and R. R. Alfano, *Phys. Rev. A* **11**, 188 (1975).

<sup>8</sup>H. Vogt and G. Neumann, *Opt. Commun.* **19**, 108 (1976).

<sup>9</sup>V. B. Podobedov, A. M. Pyndyk, and Kh. E. Sterin, *Opt. Spektrosk.* **43**, 853 (1977) [*Opt. Spectrosc. (USSR)* **43**, 504 (1977)].

<sup>10</sup>N. Bloembergen, *Nonlinear Optics*, Benjamin, New York, 1965 (Russ. Transl., Mir, M., 1966, p. 192).

<sup>11</sup>J. F. Nye, *Physical Properties of Crystals*, Clarendon Press, Oxford, 1957 (Russ. Transl., Mir, M., 1967, p. 153).

<sup>12</sup>W. D. Johnston, Jr., *Phys. Rev. B* **1**, 3494 (1970).

<sup>13</sup>A. S. Barker, Jr. and R. Loudon, *Rev. Mod. Phys.* **44**, 18 (1972).

<sup>14</sup>R. H. Pantell and H. E. Puthoff, *Fundamentals of Quantum Electronics*, Wiley, New York, 1969 (Russ. Transl., Mir, M., 1972).

<sup>15</sup>R. Loudon, *Adv. Phys.* **13**, 423 (1964).

Translated by A. Tybulewicz